Advances in Science and Technology Research Journal, 2026, 20(1), 436–450 https://doi.org/10.12913/22998624/210706 ISSN 2299-8624, License CC-BY 4.0

## Published: 2025.11.21

Received: 2025.07.26 Accepted: 2025.09.14

# Calibration and verification of the Johnson-Cook model for an austenitic steel under dynamic tension

Michał Grylewicz<sup>1</sup>

<sup>1</sup> Mechanical and Electrical Engineering Department, Polish Naval Academy, 81-103 Gdynia, Poland E-mail: m.grylewicz@amw.gdynia.pl

#### **ABSTRACT**

The paper presents the results of research on the properties of an austenitic steel used in the shipbuilding industry. Static tensile tests were conducted using an MTS testing machine, while dynamic tensile tests were carried out with rotary hammer at strain rates ranging from 250 to 2100 s<sup>-1</sup>. The obtained results were used to calibrate a Johnson-Cook model and the corresponding failure parameters suitable for finite element method (FEM) analysis. This model was then used to simulate the response of the specimen subjected to impact loading at various strain rates.

**Keywords:** austenitic steel, static tensile test, dynamic tensile test, rotary hammer, plastic characteristics, strain rate, material model in terms of FEM, CAE.

#### INTRODUCTION

In today's reality, conducting numerical simulations has become a standard in the process of creating modern structures. They allow us to customise the entire structure to predictable operating conditions, as well as optimise our product at the construction stage.

Numerical simulations owe their popularity primarily to the speed of obtaining relatively accurate results, which would be time-consuming to obtain by the analytical method and costly to obtain by the experimental method.

The notion of dynamic processes, due to its complex nature, is highly demanding. Therefore, extensive and reliable material studies are a key element. An appropriate description of material properties enables numerical simulations to be carried out as close as possible to reality, while minimising errors in the obtained results.

The Johnson-Cook (JC) model remains a standard for describing the response of metals under large strains, high strain rates, and elevated temperatures. However, its parametrisation and reliability are still the subject of intensive research. For structural steels, Yendluri et al.

(2023) presented a complete identification of the ten JC parameters (strength and damage) for E250 steel, covering an extensive experimental programme (quasi-static tests, Split Hopkinson Pressure Bar (SHPB), a range of stress triaxialities  $\eta_{\text{TRMX}}$  and temperatures) and rigorous validation with independent tests, underscoring the need for a holistic approach to model calibration in impact and blast applications [1]. In parallel, comparisons and modifications of the JC formulation are being pursued. For tool steels, it has been shown that a modified JC (MJC) and Arrhenius-type models can outperform the classical JC across broad thermomechanical regimes, especially where strain- or thermal-softening strongly affects the flow stress [2]. In aluminium matrix composites, where degradation leads to softening, it has been proposed to augment JC with a damage-induced softening term, improving agreement with  $\sigma$ - $\varepsilon$  curves at high strain rates [3]. For austenitic steels, Jiang et al. (2024) performed an inverse identification of JC parameters for 304 steel using genetic algorithms and 3D cutting simulations, showing that application-driven optimisation (process-loading conditions) can substantially reduce force-prediction

errors and better reflect service conditions than parameters obtained solely from quasi-static/ SHPB tests [4]. Taken together, these studies confirm that JC identification should span the full strain-rate range relevant to the intended application, along with the corresponding temperatures. Moreover, model modifications or extensions of damage evolution are often necessary when softening is observed. Additionally, in the work of Guo and Nemat-Nasser on Nitronic-50 steel, based on uniaxial compression tests, a strong dependence of the flow (yield) stress on strain rate (up to  $\sim 8 \times 10^3 \text{ s}^{-1}$ ) and temperature (77-1000 K) was demonstrated, including the presence of dynamic strain ageing (DSA) in the range 400-1000 K (most pronounced at low rates and diminishing at higher rates), as well as an increasing role of viscous resistance to dislocation motion at  $\dot{\varepsilon} = 10^3 \, \text{s}^{-1}$ . The authors also distinguished adiabatic and isothermal responses at high rates, confirmed by measuring and analyzing differences in the stress-strain curves[5]. Against this backdrop, the present work provides a set of JC parameters for an austenitic steel over the strain-rate range relevant to rapidly changing processes (impacts, wave interactions), together with combined numerical-experimental validation aimed at finite-element (FE) applications and may serve as a basis for follow-on studies involving comprehensive parameter identification across other stress states and temperatures.

Despite major advances in constitutive modelling of materials, physics-based models are still insufficiently advanced to capture the full complexity of the dynamic response of metals.

The present study addresses this need by focusing on an austenitic steel used in ship structures and presenting a consistent calibration and verification workflow for FE applications. The novelty lies in the use of a unique rotary-hammer test rig to perform dynamic tension over a wide strain-rate range of 250-2100 s<sup>-1</sup>, which bridges the measurement gap between classical quasi-static testing and very high rates, while better reflecting the service conditions of thin-walled hull components. From a marine applications viewpoint, the calibrated JC model is directly useful for analyses of structural resistance to impact and shock loading. A consistent perspective is presented in [6], where the Johnson-Cook model was also used to describe a non-magnetic steel and the dynamic characteristics were obtained from static and dynamic tests.

Austenitic steels owe their popularity to properties such as corrosion resistance, high strength at relatively low weight and, above all, amagnetism [7–9]. Due to these properties, they are widely used in the chemical, energy, medical, aerospace and food industries [7–10]. Austenitic steels are also increasingly used in the defence industry, especially in the construction of modern mine destroyers (Figure 1) and submarines. The reason for this is the demanding environmental conditions, such as high humidity, elevated temperatures and the impact loads caused by the detonation of explosive charges for which the strain rates reach over 10<sup>4</sup> s<sup>-1</sup> [6, 8, 11–15].

In response to the increasing use of austenitic steels in the marine industry, especially in the context of military structures, static and dynamic material tests were carried out to determine the material characteristics in the Johnson-Cook model. A properly developed model allows for implementation in numerical simulations using the finite element method, providing an effective tool for assessing the resistance of structures, especially in the context of ship hulls. Computer simulations enable the conducting detailed analyses of resistance to impact loads, providing an alternative to risky physical experiments that would involve high costs and potential damage to the test object, thus generating significant economic losses.

### MATERIAL AND SAMPLES FOR TESTS

Standardised specimens were prepared from austenitic steel material for quasi-static tensile tests on a MTS 810-02 tensile testing machine according to PN-EN ISO 6892-1:2020-5 [17] (Figure 2a). Austenitic steel is suitable for contact with seawater. It is characterised by its non-magnetic properties and resistance to intergranular corrosion [7–9, 11]. To perform the dynamic tensile test on a rotary hammer, threaded circular specimens were made with a working-part diameter of 5 mm and a length of 40 mm (Figure 2b).

### Static tensile test

After preparing the specimens and collecting initial measurements, in accordance with the norm (Figure 3) the steel specimens – with a cross-sectional area of 8 mm<sup>2</sup> and an original gauge length of 40 mm -were subjected to static tensile test



Figure 1. German Frankenthal class mine destroyer made of austenitic steel [16]



Figure 2. Specimens of tested steel for a) static and b) dynamic tests

and based on the results obtained, nominal stress-strain diagrams were created, taking into account the constant cross-sectional area of the specimen – S<sub>o</sub> throughout the whole process (Figure 4).

Based on the results obtained, a Young's modulus of E=191.87 GPa was determined in the elastic range. In addition, the nominal values of the conventional yield strength  $R_{\rm e}$  of 980 MPa and the tensile strength  $R_{\rm m}$  of 1080 MPa can be estimated.

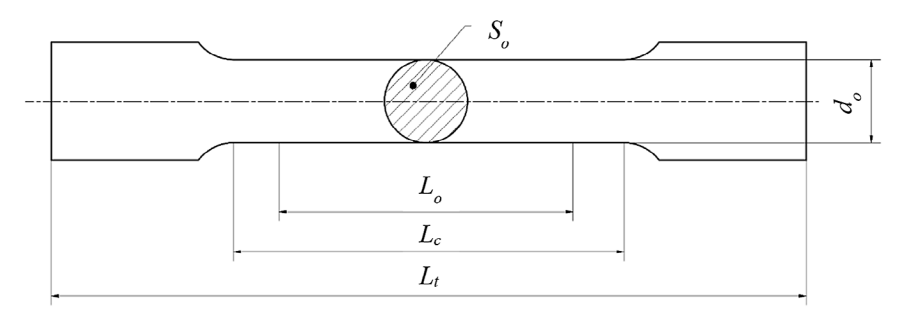
### Test of dynamic mechanical properties on a rotary hammer

The plastic behaviour of the material under short-duration deformation was investigated using a unique rotary hammer station located at the Laboratory of Fundamentals of Technology at the Polish Naval Academy. The device (Figure 5) enables the acceleration of the flywheel to a peripheral linear velocity ranging from 10 to 50 m/s. The strain rate is determined as the ratio of the specimen's fracture velocity to its gauge length [12, 15, 18].

$$\dot{\varepsilon} = \frac{\mathrm{d}\varepsilon}{\mathrm{d}t} = \frac{\mathrm{d}}{\mathrm{d}t} \left( \frac{v \cdot t}{l} \right) = \frac{v}{l} \tag{1}$$

Summarizing the above, for a specimen with a gauge length of 20 mm, the corresponding strain rates achieved range from 250÷2100 s<sup>-1</sup>.

The instrumentation integrated with the rotary hammer stand captures the fracture force of the specimen at strain rates ranging from 250 to 2100 s<sup>-1</sup>. These measurements are subsequently used to calculate the true stress values associated with the ultimate tensile strength –  $R_{\rm m, true}$  (Table 1).



 $S_o$  – original diameter of the parallel length of circular test specimen;

 $L_c$  – parallel length;

 $L_o$  – original gauge length;

 $L_t$  – total length of test specimen;

 $d_o$  – original cross-sectional area of the parallel length.

Figure 3. Initial measurements for circular specimens

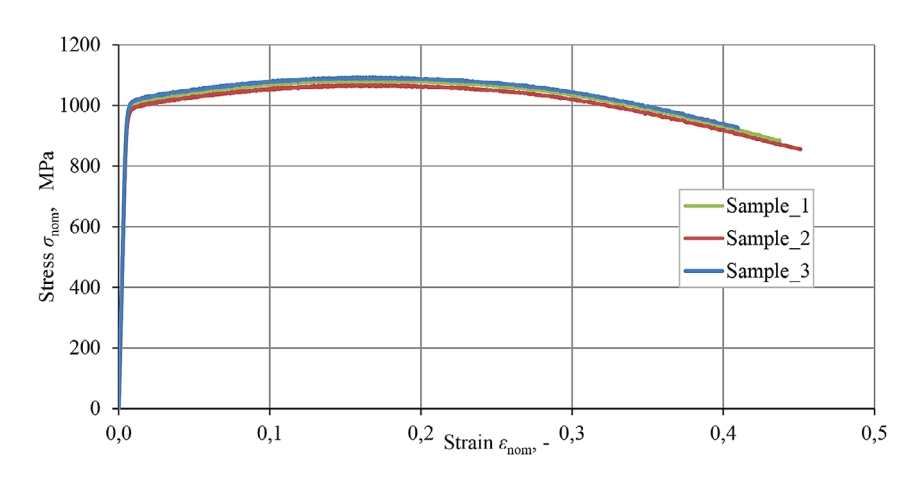
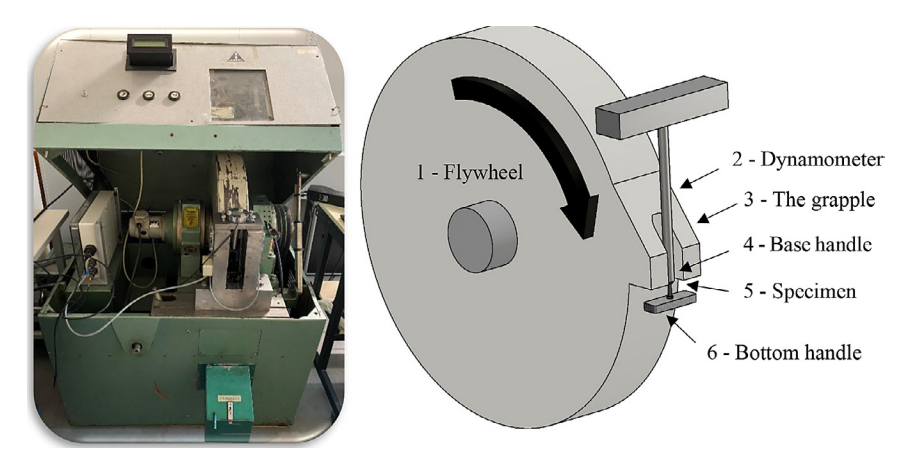


Figure 4. The results of tensile test – nominal charts of tested steel



**Figure 5.** Rotary hammer test stand and its main components: 1 – flywheel, 2 – dynamometer, 3 –grapple, 4 – base handle, 5 – specimen, 6 – bottom handle

### True characteristics as a function of plastic strain in austenitic steel

The relationship between the true stress  $\sigma_{_{true}}$  and the nominal stress  $\sigma_{_{nom}}$  is derived from the assumption that the volume of the tensile

specimen remains constant under tension, such that  $l_0 A_0 = l A(F)$ . Hence

$$\sigma_{\text{true}} = \frac{F}{A(F)} = \frac{F}{A_0} \frac{l}{l_0} = \sigma_{\text{nom}} \left(\frac{l}{l_0}\right)$$
 (2)

| The state of the s |      |                           |                      |                                   |  |                 |  |
|--|------|---------------------------|----------------------|-----------------------------------|--|-----------------|--|
| Specimen<br>designation  | φ    | Measuring Length, $L_0$ , | Area, A <sub>0</sub> | Breaking<br>Force, F <sub>m</sub> | Hammer Rotational<br>Speed, <sub>miota</sub> | Strain Rate     | True Dynamic<br>Ultimate<br>Strength, R <sub>m, true</sub> |
| 3  | mm   | mm                        | mm²                  | kN                                | m/s  | S <sup>-1</sup> | MPa  |
| Specimen_1   | 4.92 | 19.97                     | 19.00                | 40.00                             | 5  | 250             | 2105.263   |
| Specimen_2   | 4.94 | 18.82                     | 19.16                | 41.60                             | 10   | 530             | 2171.19  |
| Specimen_3   | 5.1  | 18.35                     | 20.42                | 45.00                             | 15   | 815             | 2203.722   |
| Specimen_4   | 5.05 | 16.26                     | 20.02                | 48.88                             | 30   | 1845            | 2441.558   |
| Specimen_5   | 4.94 | 19.08                     | 19.16                | 49.20                             | 40   | 2095            | 2567.85  |

**Table 1.** Overview of results obtained from rotary hammer tests

Since

$$\frac{l}{l_0} = 1 + \varepsilon_{\text{nom}} \tag{3}$$

Therefore

$$\varepsilon_{\text{true}} = \ln(1 + \varepsilon_{\text{nom}})$$
 (4)

$$\sigma_{\text{true}} = \sigma_{\text{nom}} (1 + \varepsilon_{\text{nom}})$$
 (5)

The true strain  $\epsilon_{true}$  is composed of the sum of the elastic strain  $\epsilon_{el}$  and the plastic strain  $\epsilon_{pl}$ . Consequently, the plastic strain can be expressed as follows:

$$\varepsilon_{\rm pl} = \varepsilon_{\rm true} - \varepsilon_{\rm el} = \varepsilon_{\rm true} - \frac{\sigma_{\rm true}}{E}$$
 (6)

where: F – tensile force applied to the specimen, A(F) – current cross-sectional area,  $A_{\theta}$  – original cross-sectional area in the gauge section, l – current gauge length,  $l_{\theta}$  – original gauge length,  $\varepsilon_{nom}$  – nominal strain, E – Young's modulus.

Using the above equations, the true and plastic stress-strain curves were determined for the tested specimens of the investigated austenitic steel (Table 2) (Figure 6, 7).

Based on the material properties and the intended service conditions of the austenitic steel under investigation, a review of the literature [19] was conducted. It was determined that the material most similar to the one under study is an austenitic steel designated X7CrNiAl17-7. The chemical composition of this material is presented in Table 3.

In CAE software, the plastic behaviour of materials is commonly described using polynomial functions, where the true stress is expressed as a function of plastic strain, strain rate and temperature  $\sigma_{\text{true}} = \sigma_{\text{true}} \left( \varepsilon_{\text{pl}}, \dot{\varepsilon}, \theta \right)$ . A widely adopted approach, describing plastic behaviour of metals, is Johnson-Cook constitutive model [18, 20], in which the plastic Huber-Mises-Hencky (HMH) reduced stresses  $\sigma_{pl}$  are described by the following equation [12, 15, 18–22]:

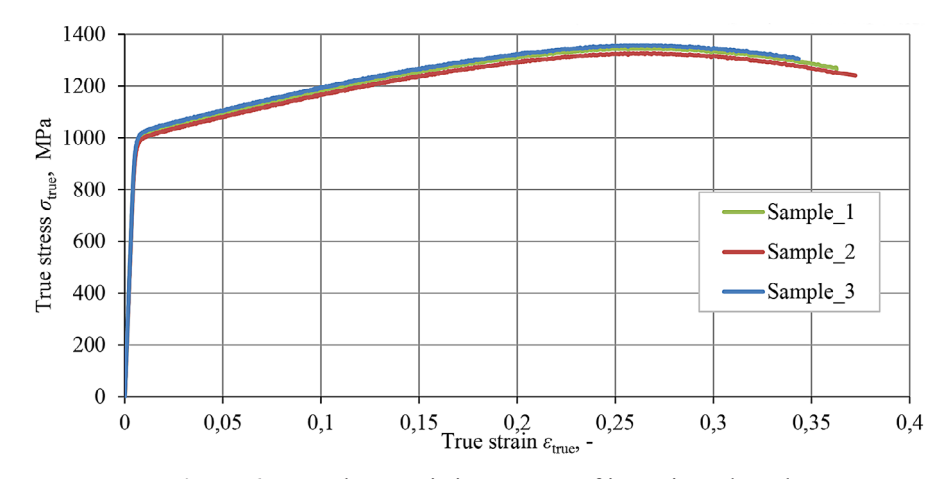


**Figure 6.** True characteristics  $\sigma_{true}$ - $\varepsilon_{rue}$  of investigated steel

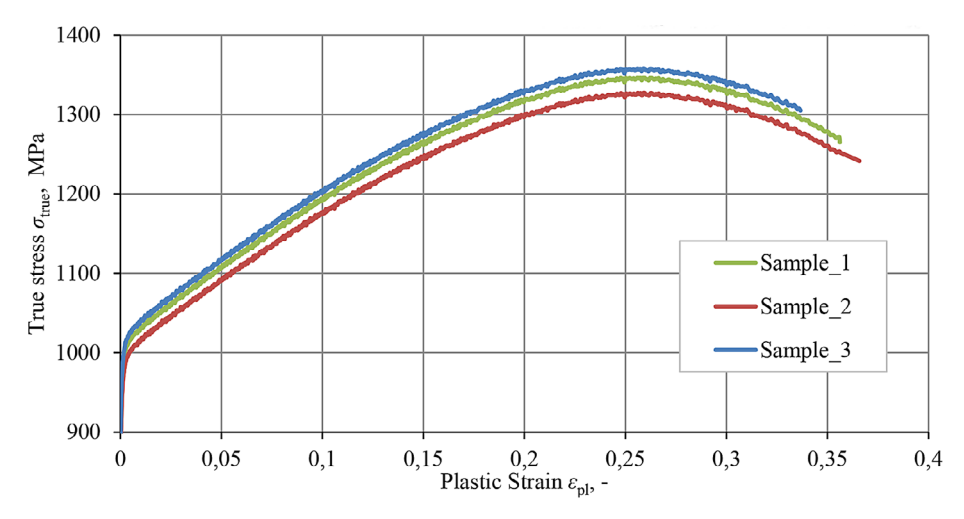


**Figure 7.** Plastic characteristics  $\sigma_{true}$  - $\varepsilon_{pl}$  of investigated steel

**Table 2.** Summary of true material properties derived from Equations 2÷6

|                    | •                  |                                     |                    |                                    |                  |                            |
|--------------------|--------------------|-------------------------------------|--------------------|------------------------------------|------------------|----------------------------|
| Sample designation | Young's<br>modulus | Conventional Yield<br>Strength (YS) | Strain at<br>YS    | Ultimate Tensile<br>Strength (UTS) | Strain at UTS    | Proportional limit         |
|                    | <i>E</i><br>GPa    | R <sub>0.002</sub><br>MPa           | ε <sub>0.002</sub> | R <sub>m</sub><br>MPa              | ε <sub>m</sub> - | A=σ <sub>p</sub> =0<br>MPa |
| Sample_1           | 191.05             | 987.80                              | 0.007              | 1346.26                            | 0.2630           | 908.02                     |
| Sample_2           | 188.93             | 980.66                              | 0.007              | 1327.22                            | 0.2620           | 895.06                     |
| Sample_3           | 195.65             | 1003.20                             | 0.007              | 1357.70                            | 0.2641           | 915.45                     |
| Average            | 191.87             | 990.55                              | 0.007              | 1343.87                            | 0.2630           | 906.18                     |

**Table 3.** Percentage chemical composition of austenitic steel X7CrNiAl17-7 [19]

| - |           |          | -           |           |            |          |            |            |
|---|-----------|----------|-------------|-----------|------------|----------|------------|------------|
|   | С         | Si       | Mn          | Р         | S          | Cr       | Al         | Ni         |
|   | max. 0.09 | max. 0.7 | max.<br>1.0 | max. 0.04 | max. 0.015 | 16 to 18 | 0.7 to 1.5 | 6.5 to 7.8 |

$$\sigma_{\rm pl} = \left( \mathbf{A} + \mathbf{B} \varepsilon_{\rm pl}^{n} \right) \left[ 1 + C \ln \left( \frac{\dot{\varepsilon}}{\dot{\varepsilon}_{0}} \right) \right]$$

$$\left[ 1 - \left( \frac{\theta - \theta_{0}}{\theta_{\rm top} - \theta_{0}} \right)^{m} \right]$$
(7)

where: A – elastic range of the material  $\sigma_{pl} = 0$  (common simplification A= $R_e$ ); B – hardening parameter; n – hardening exponent; C – strain rate coefficient;  $\varepsilon_{pl}$  – true plastic strain;  $\dot{\varepsilon}$  – strain rate;  $\dot{\varepsilon}_0$  – quasi-static strain rate 0.0001 s<sup>-1</sup>;  $\theta$  – current material temperature;  $\theta_0$  – ambient temperature;  $\theta_{top}$  – melting temperature; m – thermal softening exponent.

The individual parameters of the Johnson-Cook model are determined based on experimental data. The values corresponding to the first

term of the equation are obtained from the results of static tensile tests. To identify the parameters related to the strain rate sensitivity in the second term of the model, data from rotary hammer dynamic tensile tests were utilized.

The determination of the Johnson-Cook model parameters A, B, C, n and m can be performed using several methods [23]. One commonly applied method is the so-called engineering method, in which the parameters in the first term of the model -A, B, n – are derived from static tensile test data using the following relationships:

- Based on the obtained nominal characteristic
   ε<sub>nom</sub> σ<sub>nom</sub>, parameters R<sub>m</sub>, ε<sub>m</sub>, E and as well as
   the value of parameter A indicating the end
   of the proportionality limit were determined;
- Subsequently, using Equations 4, 5 i 6  $R_{e,true}$ ,  $R_{m,true}$ ,  $\epsilon_{m,pl}$  were calculated;

$$A = \sigma_{\text{pl}=0}$$

$$R_{\text{m,true}} = R_{\text{m}} (1 + \varepsilon_{\text{m}})$$

$$\varepsilon_{\text{m,true}} = \ln(1 + \varepsilon_{\text{m}})$$

$$\varepsilon_{\text{m,pl}} = \varepsilon_{\text{m,true}} - \frac{R_{\text{m,true}}}{E}$$
(8)

Determine the parameters B and n in accordance with the specified equations;

$$n = \frac{R_{m,true} \cdot \varepsilon_{m,pl}}{R_{m,true} - A}$$

$$B = \frac{R_{m,true} - A}{\varepsilon_{m,pl}^{n}}$$
(9)

Utilizing the average values reported in Table 2, and applying Equations 8 and 9, the coefficients associated with the first term of the Johnson-Cook (JC) constitutive model were determined as follows:

$$A = 906.18 \text{ MPa}, B = 1277.32 \text{ MPa}, n = 0.786$$

Using the aforementioned values, the true characteristic was compared with the JC model prediction as shown in Figure 8.

Owing to significant discrepancies between the true characteristic and the JC model predictions, it was necessary to revise the parameters of the first term of the constitutive equation. The yield strength was adopted as parameter A, while the remaining coefficients were recalculated using Equations 9. As a result, agreement between the true curve and the JC model improved substantially, with a maximum deviation of approximately 6.3% (Figure 9).

The averaged true stress–strain data from the examined cases were used to plot the linear relationship for  $\ln (\sigma - A)$  in accordance with equation (10). A linear regression model was fitted to the data, as shown in Figure 10.

$$\ln(\sigma - A) = n \ln \varepsilon + \ln B \tag{10}$$

A coefficient of determination (R<sup>2</sup>) exceeding 0.976 was obtained for the final linear fit (Figure 10), indicating excellent agreement between the regression model and the data.

Finally, the coefficients for the first term of the Johnson–Cook constitutive model were determined from the data in Table 2 using Equation 9, as follows:

$$A = 990.55 \text{ MPa}, B = 1095.803 \text{ MPa}, n = 0.756$$

To determine the parameter C, it is essential to know the value of  $R_{m,true}(\dot{\varepsilon})$  corresponding to a specific strain rate. The required data were obtained through dynamic tensile testing conducted using a rotary hammer, as shown in Table 4.

By transforming Equation 11, the following expression is derived:

$$C = \left(\frac{R_{\text{m,true}}(\dot{\varepsilon})}{R_{\text{m,true}}(\dot{\varepsilon}_{0})} - 1\right)$$

$$/\ln\left(\frac{\dot{\varepsilon}}{\dot{\varepsilon}_{0}}\right)$$
(11)

The calculated values of the constant C are summarized in Table 4. A constant value of C = 0.044 was adopted for further analysis. Figure 11 presents the true tensile strength as a function of strain rate  $R_{\rm m,true}(\dot{\varepsilon})$ , based on the assumed value of the parameter C.

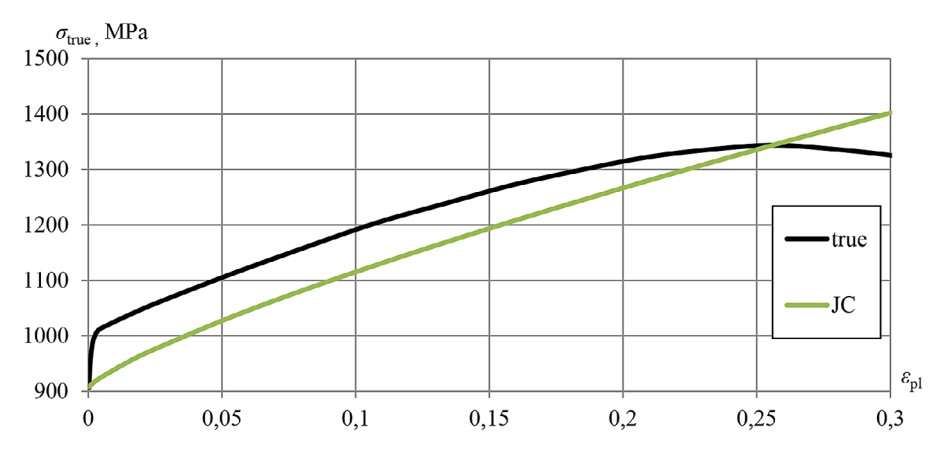


Figure 8. True characteristics and JC for the tested steel

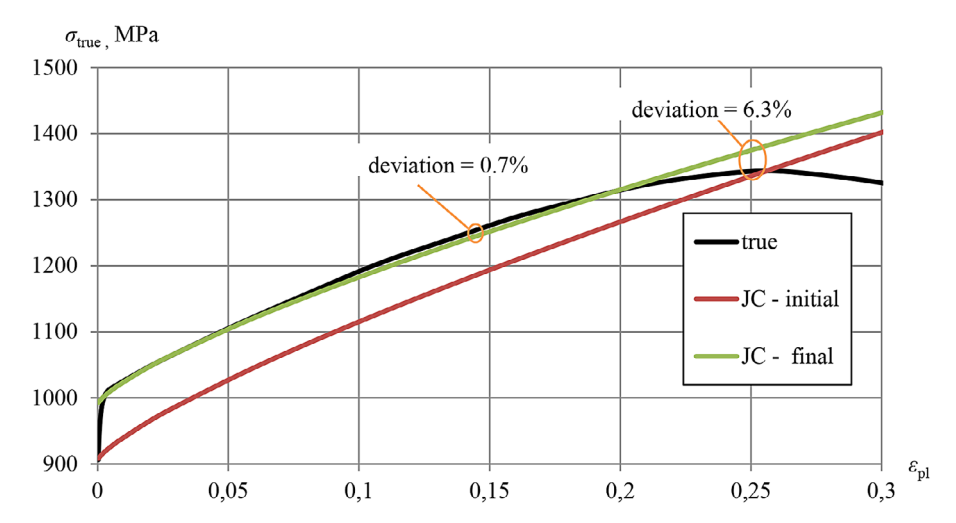
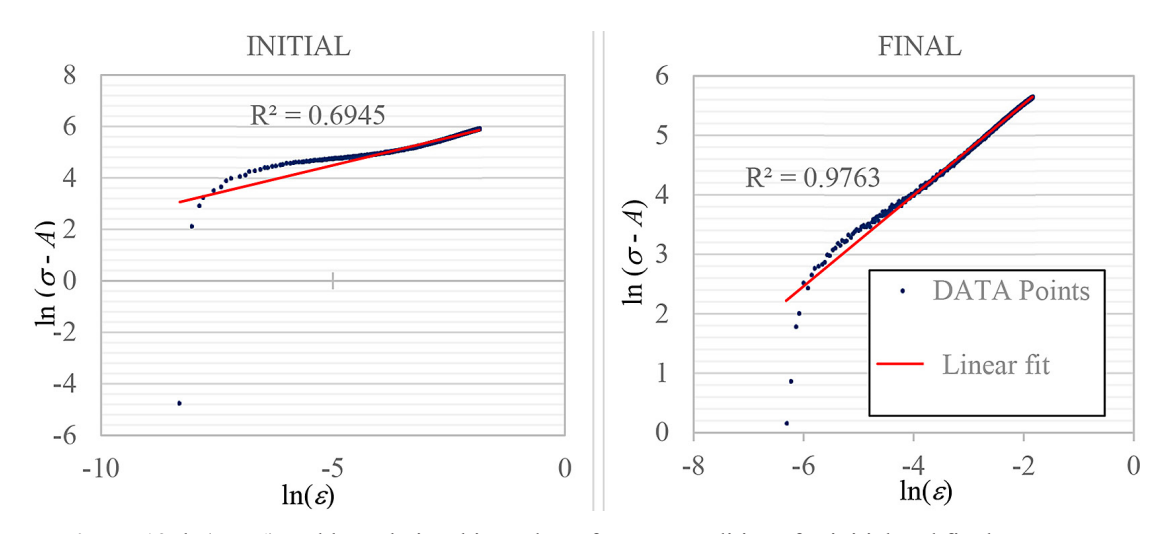


Figure 9. True characteristics with the initial and final JC model curves for the tested steel



**Figure 10.**  $\ln(\sigma - A)$  and  $\ln \varepsilon$  relationship under reference conditions for initial and final parameters

**Table 4.** Tensile strength corresponding to specific strain rates  $R_m$ ,  $\dot{\varepsilon}$ 

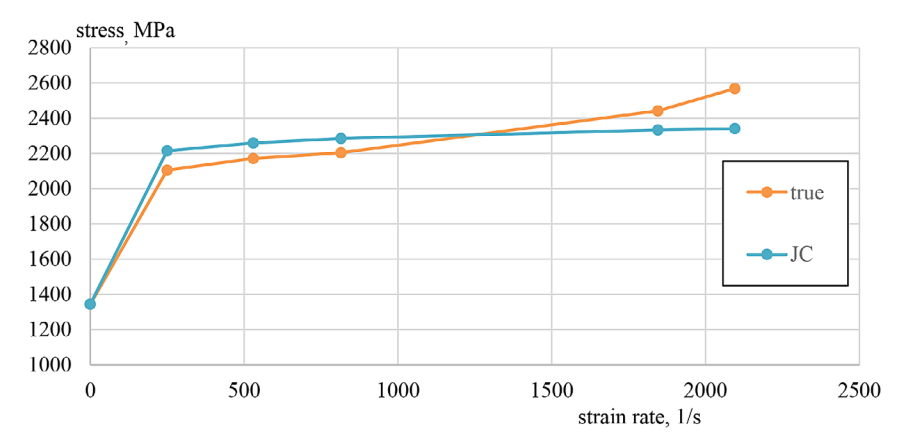
| Strain rate                                   | $\dot{\varepsilon} = 250 \text{ s}^{\text{-1}}$ | $\dot{\varepsilon} = 530 \text{ s}^{-}$ | $\dot{\varepsilon} = 815 \text{ s}^{-1}$ | $\dot{arepsilon}=1845~\mathrm{s}^{	ext{-}1}$ | $\dot{\varepsilon} = 2095 \text{ s}^{-1}$ |
|---|---|---|--|--|---|
| $R_{\mathrm{m,true},\dot{\varepsilon}}$ , MPa | 2105.04   | 2171.55                                 | 2203.95                                  | 2441.62                                      | 2568.28                                   |
| Coefficient C                                 | 0.03844754                                      | 0.039778                                | 0.040217503                              | 0.048824221                                  | 0.054047125                               |

Figure 12 compares the JC plastic characteristics as a function of strain rate for the selected value of the strain rate coefficient C.

Figure 12 shows the influence of the Johnson–Cook strain-rate coefficient C on the material response as a function of strain rate, considering the first and second terms of Equation 7 and compares this with the experimental true stress–strain characteristic derived from Equation 5. The separation between the curves corresponding to different strain rates is approximately constant with plastic strain, which correctly reflects the trend

and scale of the strain rate effect, shifts the curves toward higher stress values.

The third term of the equation accounts for the influence of temperature on the material's plastic behaviour. To determine the parameter m, static tensile tests should be conducted at elevated temperatures to obtain the tensile strength at the test temperature  $R_{\rm m}(\theta)$ . In addition, the material's melting point,  $\theta_{\rm top,}$  is required. The required values were obtained from the literature [24–27]. The following values were selected for the analysis:



**Figure 11.** True tensile strength  $R_m$  as a function of strain rate for C = 0.044

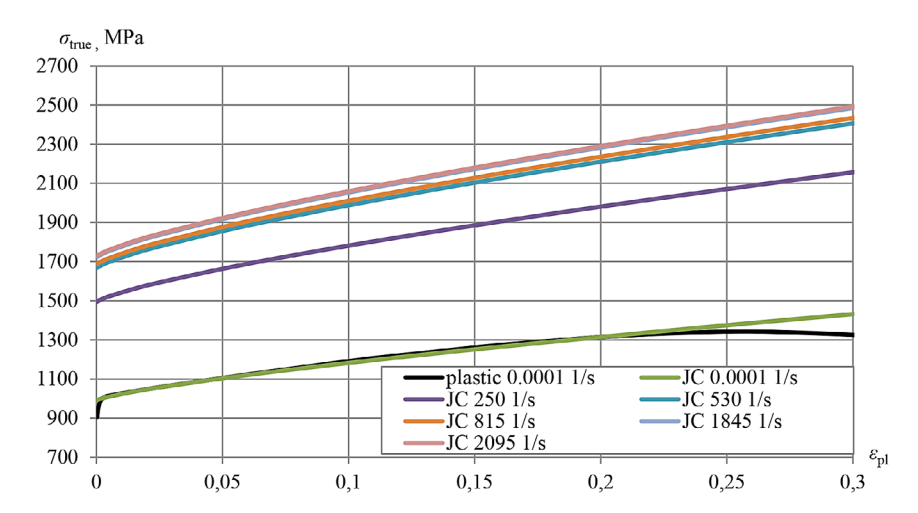


Figure 12. JC Model for austenitic steel as a function of strain rate with C = 0.044

Melting point  $\theta_{top} = 1653.15$  K; Tensile strength  $R_m = 648$  MPa at a temperature of 698.15K; Tensile strengt  $R_m = 469$  MPa at a temperature of 1003.15K.

Using the relationship between the tensile strength at elevated temperature and the tensile strength at room temperature for a strain rate of 0.0001 s<sup>-1</sup>, as defined by the following equation:

$$R_{\text{m},\theta} = R_{\text{m},0} \cdot \left[ 1 - \left( \frac{\theta - \theta_0}{\theta_{\text{top}} - \theta_0} \right)^m \right]$$
 (12)

After applying the transformation, the following expression is obtained:

$$m = \frac{\ln\left(1 - \frac{R_{\rm m,\theta}}{R_{\rm m,0}}\right)}{\ln\left(\frac{\theta - \theta_0}{\theta_{\rm ton} - \theta_0}\right)}$$
(13)

Substituting the relevant data into the equation yielded the values of the thermal plasticity

exponent *m* at the temperatures considered. These values are summarised in Table 5.

Figure 13 illustrates the temperature-dependent behaviour of the steel at strain rate of 0.0001 s<sup>-1</sup>.

### Failure model for austenitic steel

Plastic failure is governed by the existing stress state, commonly characterised by the triaxiality factor  $\eta_{TRIAX}$  [21, 28, 29]. This parameter depends on the orientation of the forces applied to the structural element. For uniaxial tension, a triaxiality factor of 1/3 was adopted [30]. The

**Table 5.** Values of parameter m calculated for selected temperatures

| Temperature, K  | Value of parameter, m |  |  |
|-----------------|-----------------------|--|--|
| 698.15 (425°C)  | 0.77                  |  |  |
| 1003.15 (730°C) | 0.88                  |  |  |
| Average value m | 0.83                  |  |  |

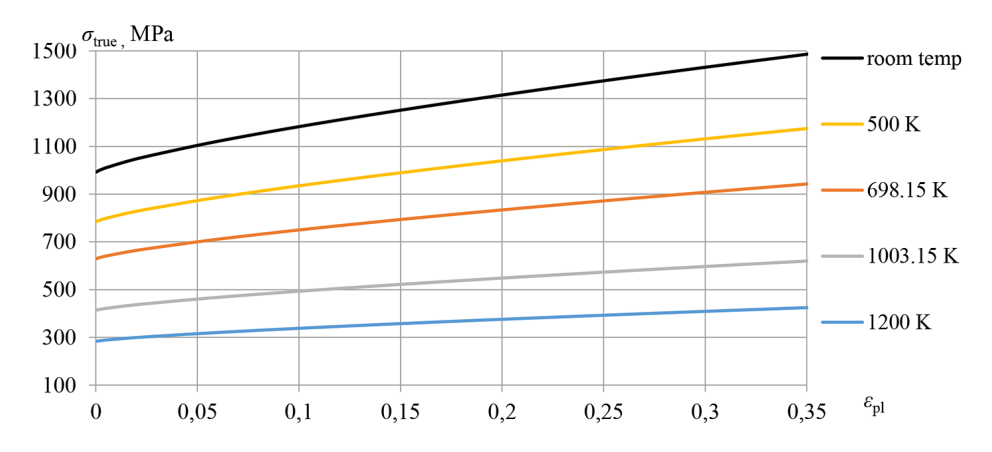


**Figure 13.** JC plasticity model as a function of temperature for  $\dot{\mathcal{E}} = 0.0001 \text{ s}^{-1}$ , A = 990.55 MPa, B = 1095.803 MPa, n = 0.756, m = 0.83

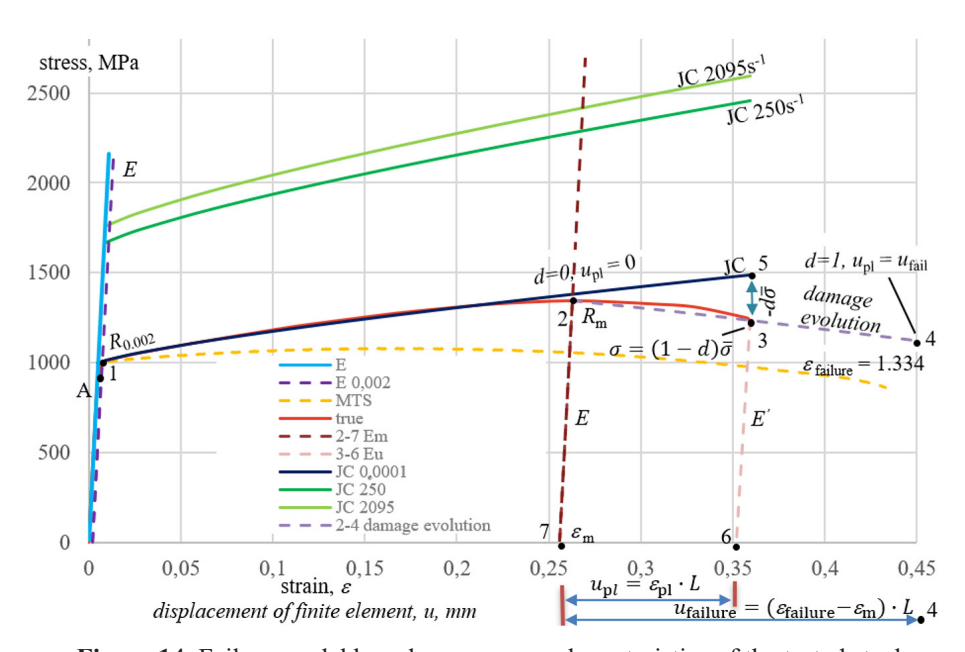


**Figure 14.** Failure model based on  $\sigma_{\text{true}}$  -  $\varepsilon_{\text{true}}$  characteristics of the tested steel

damage model was developed from the true stress-strain  $\sigma_{\text{true}}$  -  $\epsilon_{\text{true}}$  characteristics, as shown in Figure 14, using the data in Table 6.

A schematic of the material damage mechanism is shown in Figure 14. Segment 0–1 represents the elastic range, whereas the curve between points 1 and 2 represents the plastic range with hardening. Damage initiates at point 2. In a model without damage the response would continue along the hardening curve to point 5, with stress increasing monotonically with strain. Unloading from point 2 produces an elastic response, reducing the strain to point 7 along a line parallel to segment 0–1. In the model with damage, the analogue of point 5 is point 3, located on the 2–4 curve, along which a loss of strength

– referred to as softening – occurs. The 2–4 curve is called the degradation (damage) curve. It defines the parameter d, a damage-evolution coefficient taking values from 0 to 1, and the stress on this curve is given by:

$$\sigma = (1 - d)\bar{\sigma} \tag{14}$$

Complete material failure occurs upon reaching the failure strain  $\varepsilon_{failure}$ , corresponding to point 4 in the diagram. If rupture or unloading occurs while traversing the 2–4 curve (e.g., at point 3), the strain then decreases along path 3–6 owing to residual elastic forces. This path is not parallel to the elastic segment 0–1. Damage evolution describes the progressive degradation of

the material. The value d = 0 denotes the state at which the (flow) stress has reached the ultimate tensile strength  $R_m$ , but no degradation has occurred, whereas d = 1 corresponds to complete degradation of the material. The state of damage evolution is expressed as a function of the plastic displacement  $\mu_{nl}$ , defined as follows [24]:

$$u_{pl} = L\varepsilon_{pl} \tag{15}$$

where: *L* is the characteristic length of the FEM element.

The progression of material degradation is described by the damage-evolution coefficient. In CAE practice, three alternative formulations are commonly used: linear, exponential, and tabulated. The linear form is defined as the ratio of plastic displacement  $u_p$  to failure displacement  $u_{failure}$  [29]

$$d = \frac{u_{pl}}{u_{failure}} \tag{16}$$

Table 6 summarises the characteristic points shown in Figure 14 that were used to determine the material's failure parameters.

Determination of failure parameters for austenitic steel for  $\eta_{TRLAX} = 0.33$  (uniaxial tension) where L defines the size of the FEM mesh.

In summary, all parameters characterising the tested steel can be effectively described by the Johnson-Cook model.

$$\sigma = (990.55 + 1095.803 \cdot \varepsilon^{0.756}) \cdot \left[ 1 + 0.044 \cdot \ln\left(\frac{\dot{\varepsilon}}{0.0001}\right) \right] \cdot \left[ 1 - \left(\frac{\theta - 293.15}{1360}\right)^{0.83} \right]$$

Failure parameters: d = 0.1648 ; efailure = 1.334;  $\eta_{\text{Triax}} = 0.33$ ; A = 990.55 MPa; B = 1095.803 MPa; n = 0.756; m = 0.83; C = 0.044;  $\theta_0 = 293.15$  K;  $\theta_{\text{top}} = 1653.15$  K; Young's modulus  $-E = 1.91\cdot10^{11}$  Pa; Poisson's ratio -v = 0.28; Density  $-\rho = 7880$  kg/m³; Ultimate tensile strength  $-R_{\text{m}} = 1343.87$  MPa; Yield strength  $-R_{\text{c}} = 990.55$  MPa.

### Reproduction of the experiment using numerical simulation

Based on the calibrated material parameters, a numerical analysis was performed using the ABAQUS – Dynamic Explicit procedure to compare the experimental results with the simulation responses. The specimen geometry from the rotary hammer was accurately reproduced using 62,510 linear eight-node hexahedral elements, defined by 67,402 nodes. The characteristic element size was

$$\varepsilon_{\text{failure}} = \varepsilon_4 - \varepsilon_7 = 1.59 - 0.256 = 1.334$$
 
$$d\bar{\sigma} = \sigma_5 - \sigma_3 = 1478.69 - 1234.97 = 243.72 \text{ MPa}$$
 since 
$$\sigma = (1 - d)\bar{\sigma} \text{ so}, \qquad d = 1 - \frac{\sigma}{\bar{\sigma}} = 1 - \frac{1234.97}{1478.69} = 0.1648$$
 
$$E' = (1 - d)E = (1 - 0.1648) \cdot 191.87 = 160.24 \text{ GPa}$$
 
$$u_{failure} = 1.334 \cdot L$$

Table 6. Summary of values used to calculate failure parameters based on Figure 14

| Point No. | Strain            | Stress                      | Description   |  |
|-----------|-------------------|-----------------------------|---|--|
| Point No. | € <sub>e,</sub> - | $\sigma_{_{ m true}}$ , MPa | Description   |  |
| Н         | 0.0049            | 906.19                      | Limit of the proportionality $\sigma_{H} = \sigma_{pl=0}$         |  |
| 1         | 0.007             | 990.55                      | Yield strength $R_{\rm e.}$                                       |  |
| 2         | 0.263             | 1343.87                     | Tensile strength R <sub>m.</sub>                                  |  |
| 3         | 0.3595            | 1234.197                    | Fracture point  |  |
| 4         | 1.59              | 0.0                         | Total material degradation <i>d</i> =1                            |  |
| 5         | 0.3595            | 1478.69                     | Stress behaviour in a damage-free material model                  |  |
| 6         | 0.3517            | 0.0                         | Strain after fracture   |  |
| 7         | 0.256             | 0.0                         | Strain after reaching the ultimate tensile strength $R_{m,d} = 0$ |  |

set at L = 0.5 mm. The following boundary conditions were applied: the upper end of the specimen was fully fixed in all degrees of freedom, while the lower end was constrained against lateral displacements and subjected to a prescribed axial kinematic condition to achieve the target engineering strain rate. No grips were modelled. The axial motion was applied directly to the end face of the specimen. Therefore, no surface-to-surface contact or friction was defined. The total simulated time was set as  $2 \times 10^{-3}$  s for  $\dot{\varepsilon} = 250$  s<sup>-1</sup> and 2  $\times$  10<sup>-4</sup> s for  $\dot{\varepsilon}$  = 2095 s<sup>-1</sup>. The explicit time-step size was limited by the smallest element size and the elastic (acoustic) wave propagation velocity in the tested material. In this case, the maximum time-step size was  $2.36 \times 10^{-8}$  s.

The previously developed Johnson-Cook material model, including the failure model, was assigned to the reconstructed specimen geometry. Subsequently, both static and dynamic tensile tests on the rotary hammer were simulated, applying strain rates of  $\dot{\varepsilon} = 250 \text{ s}^{-1}$  and  $\dot{\varepsilon} = 2095 \text{ s}^{-1}$ . The results for  $\dot{\varepsilon} = 250 \text{ s}^{-1}$  are presented in Figure 15.

The numerical simulation results are shown in Figure 16.

The principal stress values obtained for the simulated strain rates are consistent with those predicted by the JC model. The simulated material

strength is approximately 9% higher than the values recorded in the dynamic tensile test at a strain rate of  $\dot{\varepsilon} = 250 \text{ s}^{-1}$ , and approximately 6.5% higher than those from the static tensile test.

This discrepancy is primarily attributed to the use of an average value of the parameter C within the tested strain rate range (Figure 11), as well as geometric simplifications arising from the discretisation of the specimen. It should be noted that, in the case of static loading, a more accurate representation could be achieved by using data obtained directly from the measuring equipment of the testing machine.

Additionally, the strength of the specimen in the simulation performed at a strain rate  $\dot{\varepsilon} = 2095$  s<sup>-1</sup>, using the assumed JC model coefficients, is approximately 12% lower than the values obtained from the dynamic tensile test. As shown in Figure 16, an increase in strain rate leads to a wave-like pattern of stress propagation and noticeable heterogeneity in material hardening. Despite these dynamic effects, the results are within an acceptable range, confirming that the developed JC model is suitable for simulating more demanding structures made from the tested material.

The simulation was conducted using two different mesh discretisation methods, as illustrated in Figure 17. The choice of discretisation significantly influences the distribution

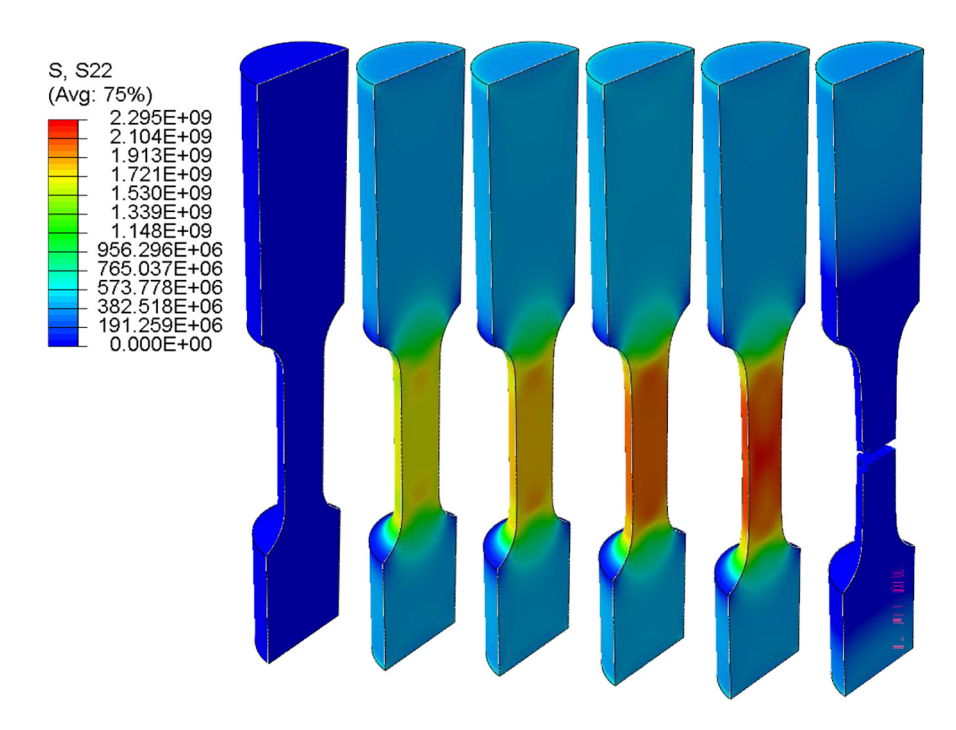


**Figure 15.** Principal stresses S22 in the tensile specimen at a strain rate of  $\dot{\varepsilon} = 250 \text{ s}^{-1}$ 

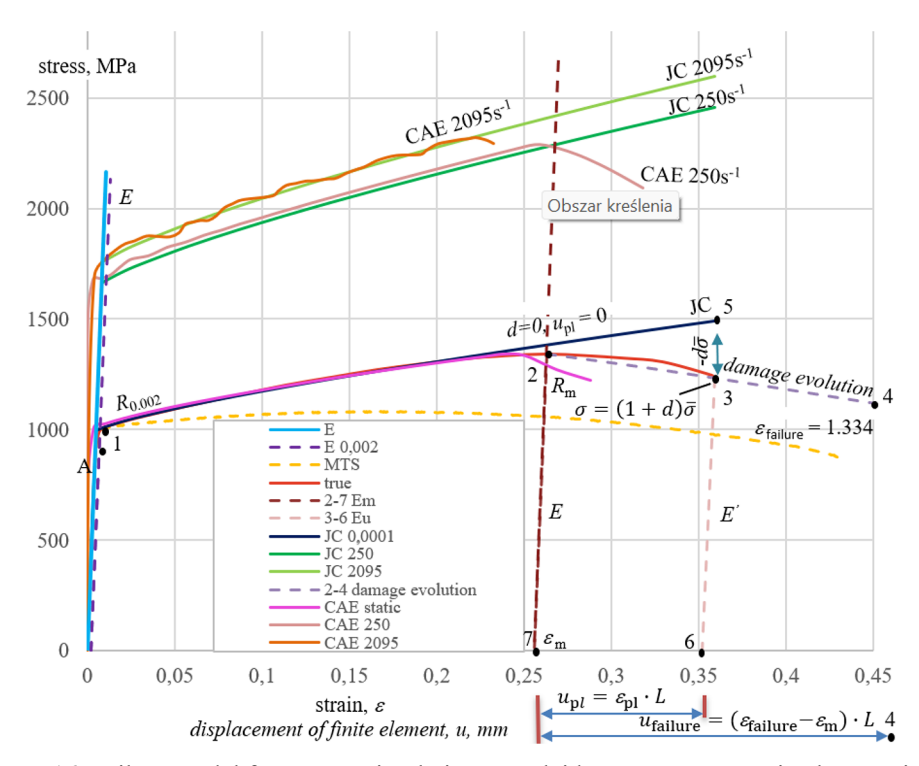
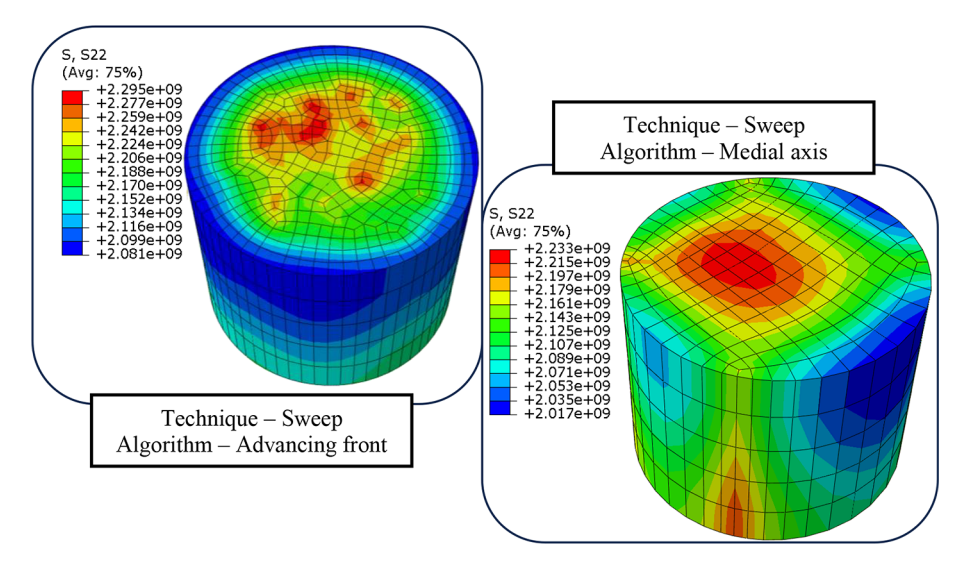


Figure 16. Failure model from CAE simulations overlaid on true stress-strain characteristics



**Figure 17.** Results for different mesh discretisation methods at a strain rate of  $\dot{\varepsilon} = 250 \text{ s}^{-1}$ 

of stress concentrations. In the case of uniaxial tension, the stress values should be relatively uniform around the entire circumference of the specimen. The observed discrepancies indicate that, for the present case, the advancing front meshing algorithm yields better agreement. This method constructs the mesh by progressively generating elements from the boundaries inward, resulting in a more uniform and physically realistic stress distribution.

### **CONCLUSIONS**

Based on static and dynamic tensile tests performed using a rotary hammer, the mechanical properties of austenitic steel were determined and a corresponding material model was developed in line with CAE software conventions for strain rates ranging from 0÷2100 s<sup>-1</sup>. This model facilitates the simulation of rapidly evolving phenomena relevant to impact events, ballistic resistance

and shock-wave effects (e.g., explosion-induced pressure) in the tested structures.

Finite element method (FEM) simulations enable the detailed calculation of field variables at any node within the analysed structure during loading. Such capabilities are essential for the accurate assessment of dynamic and high strain rate events. Moreover, reliable characterisation of the material's behaviour enables the simulations to produce results closely aligned with those obtained in physical experiments.

The comparison of numerical simulation results with experimental data demonstrated deviations of approximately 6.5%, 9% and 12% at the respective strain rates, which are within acceptable limits and confirm the validity of the developed model and its underlying material description.

The resulting material model is suitable for more complex simulations involving intricate geometries or assemblies, thereby reducing the need for costly physical crash tests during the design and development phases. This research expands the materials database for high strain-rate conditions.

Enhancement of the model's predictive reliability requires expansion of both the experimental dataset and the constitutive formulation. Results for E250 steel [1] indicate that combining tests spanning a broad range of stress triaxialities, temperatures, and strain rates - together with validation under independent loading configurations - markedly improves predictive accuracy. In the present work, the baseline Johnson-Cook model is employed, but it does not capture triaxiality-dependent void nucleation and growth or post-necking softening. Accordingly, the scope is limited to identifying damage parameters for uniaxial tension ( $\eta_{Triax}$ ). Limited material availability precluded a larger test matrix that would have enabled identification at other values of the triaxiality coefficient. Calibration and validation were carried out in uniaxial tension at a single temperature, without accounting for adiabatic self-heating at high strain rates, which affects the material response. An additional contributor to discrepancies between simulations and experiments is the adoption of a single, averaged value of the Johnson–Cook strain-rate sensitivity parameter C over the entire rate range considered. Despite these limitations, the study provides a sound basis for further work, including extension to other stress states and temperatures, explicit incorporation of thermal effects, and more precise calibration of strain-rate-dependent parameters.

#### **REFERENCES**

- Gopinath, K., Narayanamurthy, V., Khaderi, S. N., Rao, Y. V. D. Determination of parameters for johnson-cook dynamic constitutive and damage models for E250 structural steel and experimental validations, Journal of Materials Engineering and Performance, October 2024.
- Bu, H., Li, Q., Li, S., Li, M. Comparison of modified Johnson–Cook model and strain–compensated arrhenius constitutive model for 5CrNiMoV steel during compression around austenitic temperature, Journal Metals, 2022.
- 3. Chao, Z.L., Jiang, L.T., Chen, G.Q., Zhang, Q., Zhang, N.B., Zhao, Q.Q. Pang, B.J. Wu, G.H. A modified Johnson-Cook model with damage degradation for B4Cp/Al composites, Journal Composite Structures, 2022.
- 4. Jiang, X., Ding, J., Wang, C., Shiju, E., Hong, L., Yao, W., Wang, H., Zhou, C., Yu, W. Parameter identification of Johnson–Cook constitutive model based on genetic algorithm and simulation analysis for 304 stainless steel, Journal Scientific Reports, 2024.
- Wei-Guo, G., Nemat-Nasser, S. Flow stress of Nitronic-50 stainless steel over a wide range of strain rates and temperatures, Journal Mechanics of Materials, 2006.
- Szturomski, B., Kiciński, R., Milewski, S. Accelerations Caused by underwater explosions on the naval gun foundation, Advances in Science and Technology Research Journal, 2024.
- Michler, T. Austenitic stainless steels, Reference module in materials science and materials engineering, Elsevier, 2016.
- Jurczak, W. Okrętowe stale austenityczne: charakterystyka eksploatacyjna. Autobusy: technika, eksploatacja, systemy transportowe 2017.
- Ossowska, A. Wytwarzanie, budowa I właściwości warstw tlenkowych uzyskiwanych na stopach tytanu do zastosowań biomedycznych, Wydawnictwo Politechniki Gdańskiej, 2017.
- 10. Brózda, J. Stale Austenityczne nowej generacji stosowane na urządzenia energetyki o parametrach nadkrytycznych I ich spawanie; Biuletyn Instytutu Spawalnictwa w Gliwicach, 2006.
- Konieczny J., Materiały konstrukcyjne okrętów, Kwartalnik Bellona 03/2009.
- 12. Szturomski, B., Kiciński, R. Material properties of HY 80 Steel after 55 years of operation for FEM applications Materials, 2021.
- Grządziela, A., Szturomski B., Kluczyk, M. Modeling of the minehunters hull strength. Int.J.Mod. Manuf. Technol. 2012, IV.
- 14. Gong, Y., Zhang W., Du, Z., Zhu, Y. Numerical study

- on the sagging damage of the simplified hull girder subjected to underwater explosion bubble. Applied Sciences 2023, 13, 2318. https://doi.org/10.3390/app13042318
- 15. Szturomski, B. Dynamic characteristics of high quality steel in Johnson-Cook's model for fast processes simulation in CAE programs, Solid State Phenomena, 2015.
- 16. https://weaponsystems.net/system/867-Franken-thal+class
- 17. PN-EN ISO 6892-1:2020-05. Metale -- próba rozciągania Część 1: Metoda badania w temperaturze pokojowej.
- Moćko, W., Kowalewski, Z. L., Zastosowanie wybranych równań konstytutywnych do opisu właściwości mechanicznych stali wysokoazotowej typu VP159.
- Dobrzański, L. A., zespół autorów pod red. Leksykon materiałoznawstwa: praktyczne zestawienie norm polskich, zagranicznych i międzynarodowych: metale, polimery, ceramika, kompozyty, Verlag Dashofer, 2007.
- 20. Johnson, G. R., Cook, W. H. Fracture characteristics of three metals subjected to various strain, strain rates, temperatures and pressures, Engineering Fracture Mechanics, 1985; 21(1): 31–48.
- 21. Szturomski, B. The impact of non-contakt underwater explosions on the ship's hull in FEM Approach,

- Polish Naval Academy, Gdynia, 2021.
- 22. Szturomski, B., Kiciński, R. The use of Aluminium alloy after high plastic deformation for joining riveted structures, Materials, 2022.
- 23. Flis, L. Identyfikacja parametrów równania konstytutywnego Johnsona–Cook'a w odniesieniu do symulacji MES, XIII Konferencji n.t. Techniki Komputerowe w Inżynierii 2014, Licheń Stary 2014.
- Nikulin, I., Kaibyshev, R., Skorobogatykh, V. High temperature properties of an austenitic stainless steel, Journal of Physics Conference Series, August 2010.
- 25. Tehovnik, F., Arzensek, B. Arh, B. Tenisle tests on stainless steels in temperature range 800 to 1200 °C, Metalurgija, 2008.
- 26. https://www.makeitfrom.com/compare/AISI-316-S31600-Stainless-Steel/UNS-S20910-22-13-5-1.3964-XM-19-Stainless-Steel
- 27. https://www.matweb.com/search/datasheet\_print.aspx?matguid=29f84c52ec824a4ba67dbea74cbf84e6
- 28. Kohnke, P. Ansys Theory Reference, Release 5.6; ANSYS: Canonsburg, PA, USA, 1999.
- Abaqus 6.14 Theory Manual. In Simulia, Dassault Systems; Dassault Systèmes Simulia Corp.: Providence, RI, USA, 2014.
- 30. Kut, S. State of stress identification in numerical modeling of 3D issues. Arch. Metall. Mater. 2009; 54: 628–632.